Jurnal Presipitasi
Media Komunikasi dan Pengembangan Teknik Lingkungan
e-ISSN: 2550-0023

Vol 23, No 3, 2026,
Article available at homepage presipitasi

Original Research Article

Estimating Rice Crop Coefficients in Rooftop Farming Using Inverse Water and Kalman Filtering

Baskoro Tri Julianto[1,2*], Budi Indra Setiawan[3], Satyanto Krido Saptomo[3], Liyantono[4,5], Euis Kania Kurniawati[2], Muhamad Askari[6]

[1]Doctoral Program in Agricultural Engineering Science, Faculty of Engineering and Technology, IPB University, Bogor, 16680, Indonesia
[2]Department of Civil Engineering, Faculty of Science and Technology, Universitas Muhammadiyah Sukabumi, Sukabumi, 43113, Indonesia
[3]Department of Civil and Environmental Engineering, Faculty of Engineering and Technology, IPB University, Bogor, 16680, Indonesia
[4]Division of Biosystem Engineering, Faculty of Engineering and Technology, IPB University, Bogor, 16680, Indonesia
[5]Center for Environmental Research, IPB University, Bogor, 16680, Indonesia
[6]Faculty of Sustainable Agriculture, Universiti Malaysia Sabah, 90000 Sandakan, Sabah, Malaysia.
* Corresponding Author, email: 30120obaskoro@apps.ipb.ac.id

Copyright ©2026 by Authors,
Published by Environmental Engineering Department,
Faculty of Engineering, UniversitasDiponegoro
This open accessarticle is distributed under a
Creative Commons Attribution 4.0 International License

Abstract

Urban agriculture helps address land-use pressures, yet data on crop water requirements and crop coefficient (K_c) dynamics for rooftop rice cultivation remain limited. This study investigated daily K_c dynamics for IPB 3S rice grown with an automatic, non-powered fertigation system (FONi) over 100 days in Sukabumi, Indonesia. We estimated K_c using an inverse water balance that incorporated irrigation, rainfall, evapotranspiration, combined drainage and runoff, and soil water storage changes. A Kalman filter smoothed the observations, and the Verhulst logistic model tracked plant growth. Calculated K_c ranged from 0.60 to 1.09 and averaged 0.74, with the solution resting on the imposed lower bound of 0.60 on 28 of the 100 days. Sensitivity testing shows the estimates depend strongly on the unmeasured outflow term, which a 10% perturbation shifts by up to 46%. Plant growth peaked at 1.39 cm per day on the 33rd day after planting. Combining an inverse water balance with Kalman filtering and logistic growth modelling offers a workable route to daily K_c in rooftop rice systems, provided drainage and runoff are measured rather than inferred.

Keywords: Crop coefficient; inverse water balance; kalman filtering; rice growth modelling; urban farming

1. Introduction

In recent years, the agricultural sector has faced serious challenges regarding land conversion. Factors found to be influencing the conversion of agricultural land to non-agricultural use include, such as family size, potential income from agriculture and non-agricultural land use, as well as land acquisition by the state, road construction, and institutions (Quasem, 2011). It is now well established that land use changes have many negative impacts. Recent studies investigate the correlation between land use change

and the impacts of climate change. The results showed that carbon dioxide emissions would increase in regions or countries experiencing a reduction in agricultural land (Azadi *et al.*, 2021). Along with this, there is increasing concern over the decline in rice cultivation in the affected areas. A study conducted in Sigi Regency, Central Sulawesi, Indonesia, revealed that over a 10-year period, rice cultivation in the regency is predicted to decline by up to 16.5 million kg (Alamsyar, 2022). This decline is particularly critical for rice cultivation, given its role as a staple crop and its high dependence on water resources, which together highlight the need for alternative and more adaptable rice cultivation systems.

To address these challenges, agricultural innovations are needed that can change the orientation of agriculture, which was originally synonymous with cultivation on large tracts of land, to agriculture that can be practiced anywhere and anytime, without being limited by space and time. This solution can be achieved through urban farming. Urban farming is not a new concept, but rather one that has been developing for a long time and has been proven to have a positive impact on society. The literature has emphasized the importance of urban farming not solely for the urgent need for food in the face of shrinking agricultural land, but also for such as environmental conservation in urban areas, maintaining temperature and air quality, meeting economic needs, creating jobs, reducing air pollution, and driving the economy for the unemployed (Maulana *et al.*, 2022). However, urban farming systems operate under constrained rooting volume and modified microclimatic conditions, which may significantly alter crop water use patterns and complicate irrigation management relative to conventional field-based agriculture.

A growing body of literature has investigated various urban agricultural technologies, among which is Nonpowered Automatic Fertigation (in Indonesian called Fertigator Otomatis Nirdaya, FONi). FONi is a series of special pots that are connected either in series or in parallel and receive water and nutrients simultaneously from a supply tank whose water level is maintained using a float valve. This system is highly flexible and can be installed in open or controlled environments (inside greenhouses), on the ground, or in combination with other systems, provided that the water source is easily accessible to the system (Muharomah, Setiawan and Cahrial, 2023; Muharomah, Setiawan and Suwardi, 2024; Arif *et al.*, 2025). The passive and continuous nature of water and nutrient delivery in the FONi system differentiates it from conventional irrigation practices and may influence crop water uptake dynamics.

As urbanization continues to reduce the availability of cultivable land while increasing land values in metropolitan areas, rooftop agriculture has emerged as an important strategy for intensifying food production by utilizing otherwise underused building surfaces. Rather than expanding horizontally, rooftop cultivation optimizes existing urban infrastructure and offers an alternative growing space where conventional ground-level agriculture is constrained by limited land availability or soil contamination (Orsini *et al.*, 2017). Rooftop environments represent a particularly strategic spatial niche for urban agricultural intensification. In densely built cities, rooftops constitute underutilized horizontal surfaces that receive high solar exposure and minimal shading, making them thermally and radiatively suitable for crop production. At the same time, rooftops are physically separated from contaminated ground soils and urban runoff pathways, thereby reducing risks associated with heavy metal accumulation and soil-borne pathogens. From a hydrological perspective, rooftop-based systems also enable controlled water balance boundaries, since lateral subsurface flow is practically eliminated and drainage pathways can be deliberately engineered. These characteristics create a semi-closed production environment in which crop-water interactions can be monitored and managed with greater precision than in conventional ground-based plots. Consequently, integrating FONi technology into rooftop settings is not solely a spatial adaptation strategy to land scarcity, but also a methodological opportunity to investigate crop coefficient dynamics under well-defined hydrological constraints.

Previous research has demonstrated the application of FONi technology to rice cultivation under different production systems. In one study, FONi supported the cultivation of Japonica rice using the SRI-Salibu method over a 233 day growing period, producing land productivities of 2.41, 8.85, and 4.38 t ha^{-1} across three successive harvests (Safitri, 2024). Another study modified the system by replacing planting

pots with fiberglass boxes (2.00 × 1.00 × 0.40 m) for integrated rice–red tilapia cultivation. This configuration achieved a land productivity of 3.62 t ha^{-1} and estimated crop coefficients of 0.22, 1.07, 1.84, and 1.14 for the initial, vegetative, reproductive, and late growth stages, respectively (Julianto, Setiawan and Saptomo, 2024; Julianto, Setiawan, Saptomo and Liyantono, 2025; Julianto, Setiawan, Saptomo, Liyantono, *et al.*, 2025). These studies demonstrate the technical feasibility of FONi for rice production and provide preliminary crop coefficient values. However, the reported coefficients were derived from broad growth stages, implicitly assuming relatively stable water use within each stage. In fertigation-based urban farming systems, where water supply is regulated by daily water balance, evapotranspiration may fluctuate considerably, necessitating daily crop coefficient estimation.

Based on the knowledge gaps identified above, the specific objectives of this study were to: (i) develop and evaluate an inverse water balance framework for estimating daily rice crop coefficients under a passive automatic fertigation (FONi) system, (ii) improve the temporal consistency of the daily estimated K_c trajectories through Kalman filter data assimilation, and (iii) model plant height dynamics to systematically examine their temporal correspondence with daily K_c variations throughout the growth stages. By integrating inverse water balance analysis, Kalman filtering, and crop growth modelling, this study seeks to provide methodological insights into crop water use dynamics in FONi systems and improve the representation of rice water requirements under rooftop urban farming conditions.

2. Methods

2.1 Research Phases

The current investigation adopted a five-stage approach focusing on plant growth modeling and water management, which are divided into five continuous stages. The first step in this process was to collect physical data from the agricultural environment, including microclimate and plant height. These data were gathered from three main sources: weather station data to monitor temperature and humidity, sensor readings to record wind speed and rainfall, and direct field measurements to determine actual plant height. Daily and sub-daily rooftop microclimatic variables including solar radiation, air temperature, relative humidity, and wind speed were continuously monitored using an on-site Ecowitt Cellular Weather Station (Ecowitt, China). The weather station automatically transmitted recorded environmental parameters in real-time via cellular networks to a secure cloud-based data storage server. The high-frequency raw microclimatic data were subsequently retrieved for hydrological modeling by accessing the cloud telemetry database through the designated secure gateway (https://www.ecowitt.net/home/login). The raw data collected during Phase 1 was then processed to generate reference parameters based on the FAO-56 standard. At this stage, the researchers calculated evapotranspiration (ET_P) estimates using the Hargreaves method. In addition, daily rainfall modeling was conducted, along with an analysis of soil characteristics in the study area. Following the calculation of the reference parameters, the process moved to the water balance optimization phase. The researchers formulated an objective function (the mathematical optimization goal) and defined its constraints, such as the minimum and maximum soil moisture limits. The output of this phase was an estimate of a crucial parameter: the crop coefficient. In order to ensure that the resulting estimates particularly soil moisture are more accurate and have minimal reading errors, the data are processed using a 1D Kalman filter algorithm. This process involves creating a state-space representation, continuously assimilating data, and reducing noise (abnormal disturbances or fluctuations) in the soil moisture estimates. The final stage of the study comprised the integration of all the smoothed data to model plant growth. The researchers fitted the growth curves to the Verhulst logistic model. In this step, mathematical parameters were specifically determined to adjust the Crop Coefficient values for each stage of plant growth in the field. A schematic representation of this research is provided in **Figure 1.**

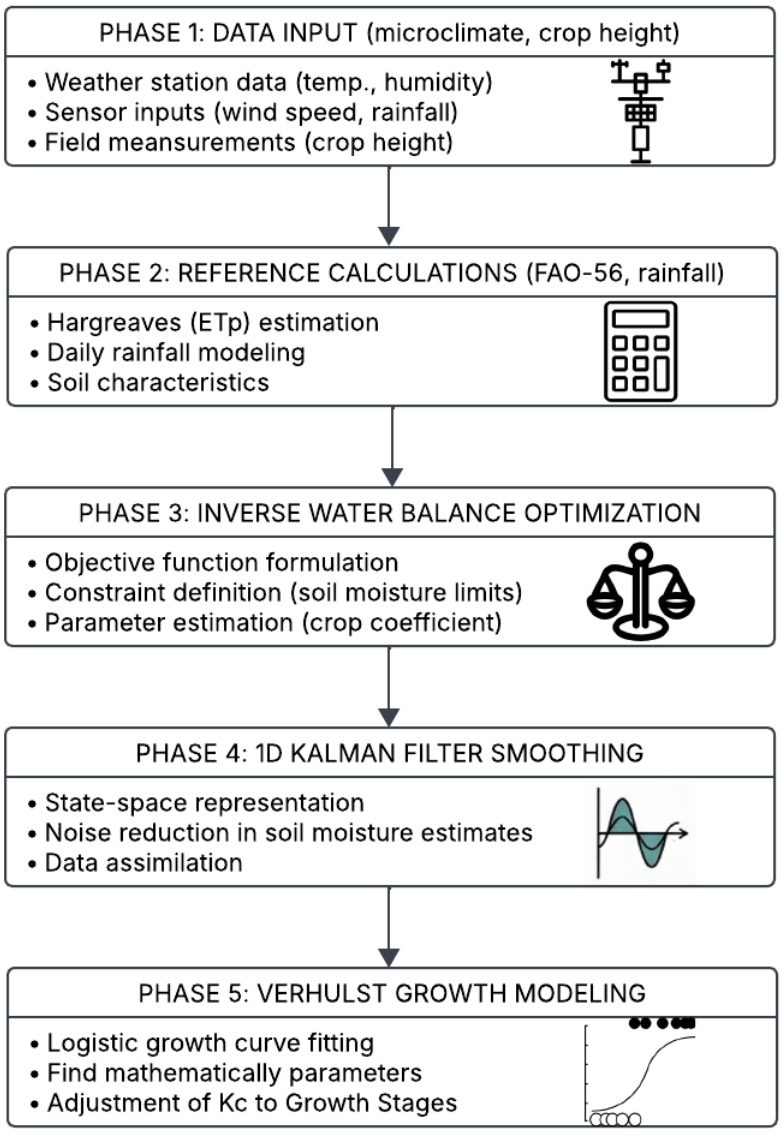


Figure 1. Research phase

2.2 Time and Place

This investigation took the form of a comprehensive experimental study conducted over a duration of 100 days, specifically from July to October 2025. The designated site for this research was the rooftop of the 4th floor of Building E at Universitas Muhammadiyah Sukabumi, providing the necessary open-air exposure for the experiment. The main campus is located at Jalan R. Syamsudi, SH , No. 50, Cikole, Sukabumi, West Java, Indonesia. For exact geographical reference, the specific coordinate point of the location was identified as 6°55'11.1"S 106°56'03.7"E.

2.3 Design and Treatment

The FONi system employed in this study comprised a series of interconnected plant pots connected to a control tank, and a nutrient tank, each of which is height-adjusted using an automatic float valve. The system consists of 24 pot sets used for rice cultivation with native paddy soil as the planting medium. The system layout used can be seen in **Figure 2** and **Figure 3**.

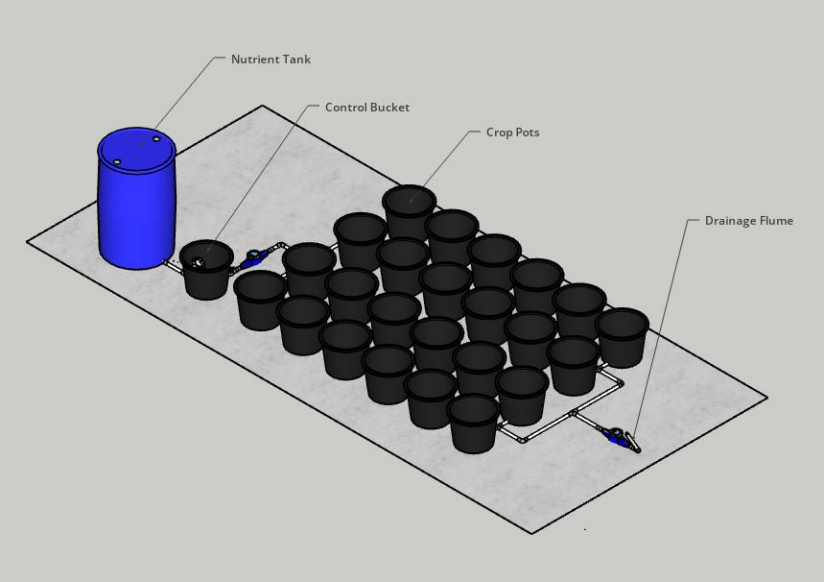


Figure 2. System layout in isometric view

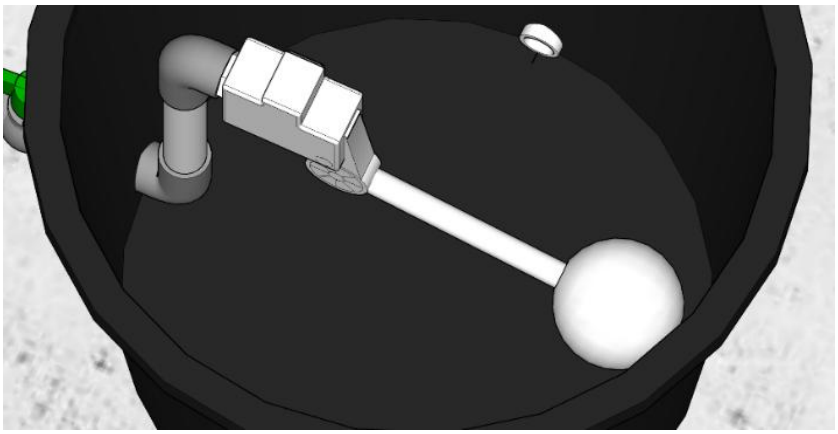


Figure 3. Automatic float valve as a water level control mechanism at control bucket

The plant pots are made of shatterproof rubber buckets with holes on one side of the base for pipe installation. The pots are arranged and assembled and connected with 1/2" PVC pipes, the water level of which is regulated by a closed control bucket and a drainage channel to counterbalance the water level in case of rain. The water level in the control bucket is set to maintain a water level of 5 cm below soil level. This value is taken because it is expected to be the optimum condition for increasing land productivity and water use efficiency (Hasanah *et al.*, 2017).

The rice used is the IPB 3S variety. IPB 3S rice is a paddy rice released by IPB University in 2014, which is claimed to have a productivity potential of 7-8 tons ha^{-1} and is claimed to have the advantage of not requiring a lot of water and urea fertilizer (Kurniawan, Kristina and Awiyantini, 2021). The rice is soaked in water for several days and then transferred to a seedling tray filled with planting media. The sowing process is carried out for seven days with a density of one seed per seedling tray hole. The seedlings are transplanted with a density of one seedling planted in one polybag in one pot. In practice, the rice plants are given liquid NPK fertilizer and AB mix at a specific dosage once a week through the nutrient tank.

2.4 Hydrological and Water Balance Analysis

Water balance analysis was a central component of the analysis conducted in this study. Water balance analysis was conducted on plant pots to observe the equilibrium of water inflow and outflow

from each system. Water balance review was only conducted on plant pots where the water inflow component consisted of irrigation water and rain, while the water outflow component consisted of plant evapotranspiration, drainage, and runoff. Mathematically, the daily water balance used can be seen in **Equation 1.**

$$I_r + R = ET_c + D_r + R_O \pm \frac{\Delta S}{\Delta t} \quad (1)$$

Variable I_r represents irrigation water (mm), R represents rainfall (mm), ET_c represents crop evapotranspiration (mm), D_r represents drainage (mm), R_O represents runoff (mm), and $\frac{\Delta S}{\Delta t}$ represents the daily change in soil water storage (mm day^{-1}). Irrigation values are obtained by measuring water meters that are read weekly to obtain weekly irrigation accumulation, which will be distributed daily.

Daily inflows and outflows in individual pots were too small to measure reliably by hand, so cumulative water use was logged every seven days using an inline mechanical flow meter. Dividing each weekly volume evenly across the seven days provided the daily irrigation rate. Because the float valves continuously replenished soil water in response to transpirational demand rather than scheduled applications, this uniform daily rate approximated actual delivery far better than it would have under intermittent manual irrigation. **Section 3.4** details the limits of this assumption.

Daily inflows and outflows in individual pots were too small to measure reliably by hand, so cumulative water use was logged every seven days using an inline mechanical flow meter. Weekly irrigation was then partitioned daily in proportion to potential evapotranspiration rather than divided evenly. Because automatic float valves replenished soil moisture continuously as the crop transpired, scaling daily inputs by atmospheric demand better reflects actual water uptake than a uniform daily average. The sensitivity of the daily K_c estimates to this temporal disaggregation method is evaluated in **Section 3.4**.

Rainfall and crop evapotranspiration values are obtained by measuring using an automatic weather station installed adjacent to the system used. Evapotranspiration is not obtained directly from the weather station but is modelled by multiplying the potential evapotranspiration value and the crop coefficient value. Empirical field measurements of crop coefficient, drainage, and runoff are difficult to obtain. Because the flow meters could not measure D_r and R_o separately, and both represent water discharging from the system, they were combined into a single outflow variable ($D_r + R_O$). Daily values for K_c and ($D_r + R_O$) were then optimized using Excel Solver. Potential evapotranspiration and water storage changes can be calculated as follows (Allen *et al.*, 1998; Hargreaves and Allen, 2003; Saptomo *et al.*, 2015; Muharomah *et al.*, 2024):

$$ET_P = 0.000939 R_a (T_a + 17.8)(T_x - T_n)^{0.5} \quad (2)$$

$$d_r = 1 + 0.033 \cos(0.0172J) \quad (3)$$

$$\varphi = \frac{\pi L}{180} \quad (4)$$

$$\delta = 0.409 \sin(0.0172J - 1.39) \quad (5)$$

$$\omega_s = \cos^{-1}(-\tan(\varphi)\tan(\delta)) \quad (6)$$

$$R_a = 37.6 d_r [\omega_s \sin(\varphi)\sin(\delta) + \cos(\varphi)\cos(\delta)\sin(\omega_s)] \quad (7)$$

$$S = \begin{cases} WL\theta_s + D, & if\ WL > Z \\ WL\theta_s + (Z - WL)\theta, & if\ WL < Z \end{cases} \quad (8)$$

$$\frac{\Delta S}{\Delta t} = S_t - S_{t-1} \quad (9)$$

Variable ET_P represents potential evapotranspiration using the Hargreaves method (mm), R_a represents extraterrestrial solar radiation (MJ m^{-2} day^{-1}), T_x represents the daily maximum temperature (°C), T_n represents the daily minimum temperature (°C), T_a represents the daily average temperature (°C), d_r represents the relative distance of the Earth to the Sun, J represents the day in the Julian calendar (its

value ranges from 1 to 366 days according to the observation date), φ represents the latitude position in radians, L represents the latitude position in degrees, δ represents the solar declination, ω_s represents the solar hour angle, S represents groundwater storage (mm), WL represents water level (mm), Z represents soil surface elevation (mm), D represents standing water depth (mm), θ represents soil moisture content (%), and θ_s represents saturated water content (%). Soil parameter measurements were taken using sensors measured from a depth of 5-15 cm from the surface of the polybag soil. Because empirical measurements of the crop coefficient and combined outflow ($D_r + R_O$) are difficult to obtain, both terms were optimized in Excel Solver. Equation 1 is modified accordingly:

$$\frac{\Delta S}{\Delta t} = I_r + R - (ET_P \times K_c) - (D_r + R_O) \tag{10}$$

Two daily parameters, K_c and combined ($D_r + R_O$), were estimated simultaneously across the 100-day series (200 decision variables total) using the Generalized Reduced Gradient (GRG) Nonlinear algorithm in Excel Solver. To avoid local optima and test parameter identifiability, Solver was configured with a Multistart routine using a population size of 100. The objective function minimized the root mean square error ($RMSE$) between observed and simulated daily changes in soil water storage. Parameter values for K_c were bounded by the FAO-56 physiological limits for rice, 0.60 to 1.20 (Allen et al., 1998), and combined drainage and runoff were constrained to non-negative values to maintain mass conservation. To test for equifinality, the optimization was repeated across five independent trials using initial states drawn randomly from a uniform distribution. Across all five trials, the solver consistently converged to an identical global optimum with an RMSE of 4.002, and the resulting daily K_c trajectories showed zero variance **(Appendix E).** This consistent convergence indicates that the estimated K_c parameters are unique and identifiable within the defined bounds, This consistent convergence indicates that the estimated K_c parameters are unique and identifiable within the defined bounds for a given outflow series. However, it does not establish that the outflow partition itself is fully identifiable.

Model performance is evaluated by comparing the observed and simulated $\frac{\Delta S}{\Delta t}$ values using the coefficient of determination (R^2) and Root Mean Square Error ($RMSE$). The R^2 value is used to measure how much of the observed variation in water storage can be explained by the model, thus indicating the degree of agreement between the simulation results and empirical data. Meanwhile, $RMSE$ is used to measure the average deviation between the simulated and observed $\frac{\Delta S}{\Delta t}$ values in the same units, thereby representing the level of model prediction error quantitatively. A model is said to have good performance if it produces a high R^2 value and low $RMSE$, indicating that the crop coefficient, drainage, and runoff parameters obtained through optimization are able to adequately represent the dynamics of water storage changes. The R^2 and $RMSE$ values can be calculated as follows (Di Bucchianico, 2007; Chicco, Warrens and Jurman, 2021; Hodson, 2022):

$$RMSE = \left(\frac{1}{n}\sum_{i=1}^{n}(y_i - \hat{y}_i)^2\right)^{0.5} \tag{11}$$

$$R^2 = 1 - \frac{\sum_{i=1}^{n}(y_i - \hat{y}_i)^2}{\sum_{i=1}^{n}(y_i - \bar{y})^2} \tag{12}$$

Model performance was evaluated using two statistical indicators, namely **Equation (11)** for $RMSE$ and **Equation (12)** for the R^2. In **Equation (11)**, RMSE is calculated as the square root of the mean of the squared differences between the simulated values $\hat{y}_i$ and the observed values y_i, where n denotes the total number of data points and i represents the observation index. The $RMSE$ has the same unit as the evaluated variable and represents the average magnitude of absolute deviation between model predictions and observations, with smaller values indicating better predictive accuracy. Meanwhile, **Equation (12)** defines R^2 as a measure of the proportion of variability in the observed data y_i that can be

explained by the model, where $\bar{y}$ denotes the mean of the observed values. The R^2 value is dimensionless and ranges from 0 to 1, with values closer to 1 indicating a higher level of agreement between the model and the observed data pattern.

2.5 Crop Modelling

Crop modelling in this study comprised two integrated components: a crop growth representation and a $K_c$estimation framework. The growth component described plant development across phenological stages to characterize temporal variations in canopy development and water demand, while the crop coefficient model was formulated using an inverse water balance approach in which K_c was treated as a dynamic parameter governing actual evapotranspiration. Because inverse water balance calculations are sensitive to uncertainties in root-zone water depletion (D_r), runoff (R_O), and other hydrological components, the estimated daily K_c values may contain stochastic fluctuations that do not necessarily reflect actual crop physiological changes. Kalman filtering is a recursive state-estimation technique that combines model predictions with observations to minimize estimation error while preserving the temporal evolution of the underlying system, making it well suited for estimating time-varying state variables from noisy observations (Simon, 2006).

In this study, the constrained optimization results were treated as observations within a state-space framework, and a Kalman filter was applied to estimate a temporally consistent daily K_c trajectory. At each time step, the filter updated the predicted K_c using observational residuals while accounting for process and measurement uncertainties. This recursive estimation reduced high-frequency fluctuations without eliminating seasonal variations associated with crop development. Kalman filtering has been widely adopted in crop-soil monitoring and irrigation applications because it provides robust estimation of dynamic state variables under uncertain measurements while preserving the temporal evolution of the system (Lopez-Jimenez, Vande Wouwer and Quijano, 2022). The filtered K_c series reflects the same inverse-balance estimates with high-frequency noise removed. While smoothing dampens day-to-day fluctuations, it introduces no new information; the resulting curve shares the uncertainty of the raw estimates and offers no independent gain in accuracy. The Kalman filtering framework is illustrated in **Figure 4.**

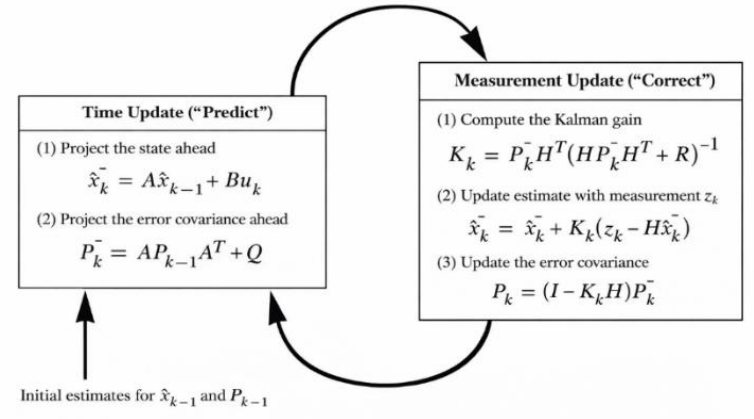


Figure 4. Kalman filter algorithm. Reproduced from (Estinigtyas, Suciantini and Irianto, 2005) under the terms of the Creative Commons Attribution 4.0 International License (CC-BY 4.0), Copyright 2005 Agromet, PERHIMPI and IPB University.

Based on **Figure 4**, the Kalman Filter operates through two recursive stages: Time Update ("Predict") and Measurement Update ("Correct"). In the Time Update step, the state is projected ahead using the system model, $\hat{x}_k^- = A\hat{x}_{k-1} + Bu_k$, and the error covariance is also projected ahead, $P_k^- = AP_{k-1}A^T + Q$, where Q represents the process noise covariance; these quantities constitute the *a priori* estimates. In the Measurement Update step, the Kalman gain is computed as $K_k = P_k^- H^T (HP_k^- H^T + R)^{-1}$,

balancing the uncertainty between the projected estimate and the measurement noise covariance R. The state estimate is then updated using the innovation (measurement residual), $\hat{x}_k = \hat{x}_k^- + K_k(z_k - H\hat{x}_k^-)$, followed by updating the error covariance, $P_k = (I - K_k H)P_k^-$. This iterative cycle continuously refines the state estimate by optimally combining model prediction and measurement information in a minimum mean square error sense under linear-Gaussian assumptions.

In this study, the process noise covariance (Q) and the measurement noise covariance (R) were both set to a balanced value of 0.001, establishing a noise covariance ratio (Q/R) of 1 (Lodh *et al.*, 2024). This parameterization strategy is scientifically justified through both biophysical and mathematical frameworks. Biophysically, the crop coefficient is strictly regulated by canopy development and leaf area index (LAI), which are gradual, continuous physiological processes (Eliades *et al.*, 2022). Consequently, day-to-day transitions in K_c are highly conservative. A low process covariance $Q = 0.001$ successfully represents this biological constraint, preventing unphysical, abrupt daily spikes in the estimated state. Mathematically, the daily 'observations' assimilated into the filter are not raw, high-frequency sensor readings, but rather optimized *Raw* K_c daily values derived from the inverse water balance closure via high-precision microclimate monitoring. Therefore, the observational noise is inherently controlled, justifying a low measurement covariance $R = 0.001$ (Drieschner, Herrmann and Petryna, 2023; Ye *et al.*, 2025). In sequential data assimilation where exact physical noise statistics are challenging to quantify a priori, maintaining $Q/R = 1$ is a standard, robust tuning practice (Weerts and El Serafy, 2006). This balanced gain ensures that the filter effectively dampens localized high-frequency microclimatic noise while remaining highly sensitive to genuine, trend-wise phenological transitions across the rice growth stages.

In addition to optimizing the K_c using an inverse water balance approach, this study models plant height dynamics to provide a biological growth reference. To monitor the biophysical development of the rice crop, plant height (cm) was measured at weekly intervals (every 7 days) from transplanting until physiological maturity at 99 days after transplanting (DAT). To eliminate sampling bias and ensure maximum statistical representation, a complete census of the experimental population was performed, wherein plant height was measured for every single cultivated plant across all pot replicates. Plant height was recorded using a standardized ruler or a vertical height measuring tool, measured vertically from the substrate surface line to the tip of the highest fully opened leaf blade, pulled gently straight to ensure consistency. Because plant height changes daily and follows a characteristic growth trajectory, it is described using the Verhulst logistic equation. The simulated plant height $y(t)$ and the optimized K_c values are subsequently presented on the same graph to examine their temporal patterns and potential correspondence, rather than to imply a direct functional relationship. The logistic equation in question can be expressed as follows (Abdul, Anuar and Mior, 2020; Ginoga and Julianto, 2025):

$$y(t) = \frac{K}{1 + Ae^{-rt}} \tag{13}$$

$$\frac{dy}{dt} = ry\left(1 - \frac{y}{K}\right) \tag{14}$$

The crop height growth model in this study is expressed using the Verhulst logistic equation, where **Equation (13)** represents plant height as a function of time and **Equation (14)** represents the rate of change of height with respect to time. In this model, $y(t)$ denotes plant height at time $t$with units of (cm), while t represents time in days after planting (days). The parameter K represents the maximum potential plant height (cm), r is the intrinsic growth rate (cm day^{-1}), and A is the integration constant, which is dimensionless. The derivative $\frac{dy}{dt}$ represents the plant height growth rate (cm day^{-1}). To parameterize the model, the parameter K was deterministically set as the actual mean plant height measured at the final day of observation (99 DAT). The parameters A and r were estimated through an optimization process using field measured plant height data (cm), with model performance evaluated based on the R^2 and $RMSE$ as presented in **Equation (11)** and **Equation (12)**.

3. Results and Discussion

3.1 Microclimate

As shown in **Figure 5** the microclimate conditions recorded by the Automatic Weather Station during the 100-day planting period. Each microclimate parameter, namely maximum daily temperature (T_x), average daily temperature (T_a), minimum daily temperature (T_n), and relative humidity (RH), shows a gradual and moderate increase as seen from the linear trend presented in the figure, with RH, T_x, T_a, and T_n at 0.01%, 0.02°C, 0.01°C, and 0.01°C per day, respectively.

Figure 5 also depicts the temporal distribution of potential evapotranspiration (ET_P) in relation to extraterrestrial solar radiation (R_a) during the 100-day planting period. The R_a curve follows a clear parabolic pattern, increasing from the early planting stage and reaching its maximum value of 37.3 MJ m^{-2} day^{-1} at Day 51, before gradually declining toward the end of the season. In contrast, ET_P shown as daily scatter points exhibit noticeable short-term variability, ranging from 2.2 to 5.2 mm day^{-1}. Most observations cluster between 3.8- and 4.9-mm day^{-1}, although a distinct mid-season dip is observed around Day 58.

Taken together, these results suggest that potential evapotranspiration (ET_P) did not increase proportionally with the seasonal peak in extraterrestrial radiation (R_a). Although slightly higher ET_P values occurred near mid-season when R_a reached its maximum, the overall variability suggests that the local rooftop microclimate exerted stronger control over the evaporative response. In rooftop cultivation systems, incoming solar radiation represents the primary energy source, but the partitioning of this energy into sensible and latent heat fluxes is strongly influenced by local atmospheric conditions, vegetation, and substrate characteristics (Cascone *et al.*, 2019; Drottberger *et al.*, 2023). Evaporation from the growing medium together with plant transpiration increases moisture in the air surrounding the canopy, thereby maintaining relatively high relative humidity and reducing the vapor pressure deficit even under increasing air temperatures (Begum *et al.*, 2021). This thermodynamic buffering limits the conversion of available radiant energy into evapotranspiration, which may explain why daily ET_P exhibited only moderate fluctuations despite the pronounced seasonal variation in R_a. Similar interactions between radiation, air temperature, humidity, and evapotranspiration have been identified as key processes governing the microclimate of rooftop agriculture systems. Consequently, while R_a defines the theoretical energy available for evaporation, the realized evapotranspiration is governed by the combined effects of air temperature, atmospheric humidity, and crop–surface energy exchange within the rooftop environment. These localized microclimatic processes distinguish rooftop cultivation from conventional ground-based systems and reinforce the need for site-specific crop coefficient (K_c) estimation.

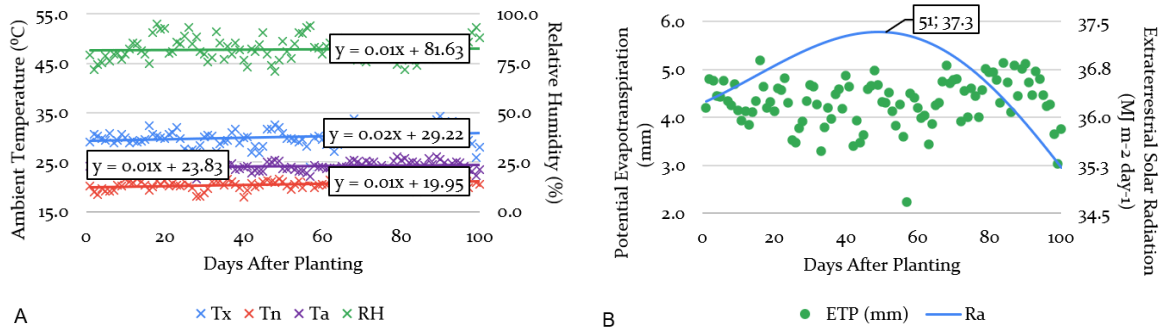


Figure 5. Temporal variation of potential evapotranspiration and extraterrestrial solar radiation during the 100-day planting period. (A) Daily microclimate recorded. (B) Potential evapotranspiration estimation and solar radiation

3.2 Soil Water Condition

Water conditions in the soil were monitored daily. **Figure 6** shows the dynamics of groundwater storage in the system. Due to the destructive nature of direct porosity sampling which could disrupt the continuous operation of the FONi system and the established root zone, total porosity was approximated at 68%. This value is representative of general porosity in paddy top soils (Aimrun, Amin and Eltaib, 2004). An inspection of the data reveals that no water level measurements were taken from day 1 after planting to day 37 after planting. This missing data could be attributed to ongoing adjustments to the measuring equipment. To address this data gap, the water level during this period was set equal to the design water level, which is 210 mm from the bottom of the pot or -50 mm from the surface of the soil in the polybag.

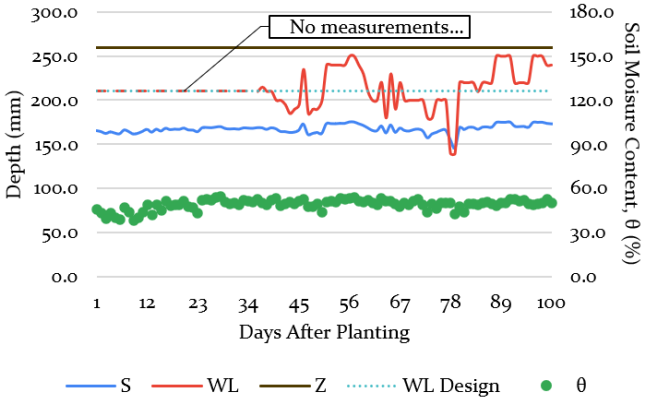


Figure 6. Soil water dynamic

Based on **Figure 6**, during the first 37 days after planting, WL was fixed at the design level (210 mm), resulting in nearly constant S. This imposed boundary condition produced a stable storage regime during the early growth stage. After measurements resumed, exhibited noticeable fluctuations in WL, which directly altered the saturated storage component $WL\theta_s$. However, θ remained relatively stable throughout the observation period, indicating that variations in S were primarily controlled by changes in WL rather than changes in θ. Although WL fluctuated during the later stages of observation, the resulting changes in S were mainly associated with variations in the saturated zone thickness. Since θ did not approach θ_s at any time, the soil profile did not reach full saturation throughout the observation period. This indicates that the root zone predominantly remained under unsaturated conditions, even when WL was maintained at -50 mm relative to the soil surface. Consequently, changes in S were governed primarily by fluctuations in WL rather than by significant changes in volumetric soil moisture θ.

3.3 Inverse Water Balance Analysis and Crop Coefficient Estimation

Figure 7 illustrates the dynamics of changes in soil water storage based on both mathematical calculations (calculated from empirical data) and inverse water balance optimized using a solver. In system, the relationship between changes in soil water storage based on mathematical calculations and inverse water balance has a deterministic coefficient value of 0.29 and an $RMSE$ of 4.002.

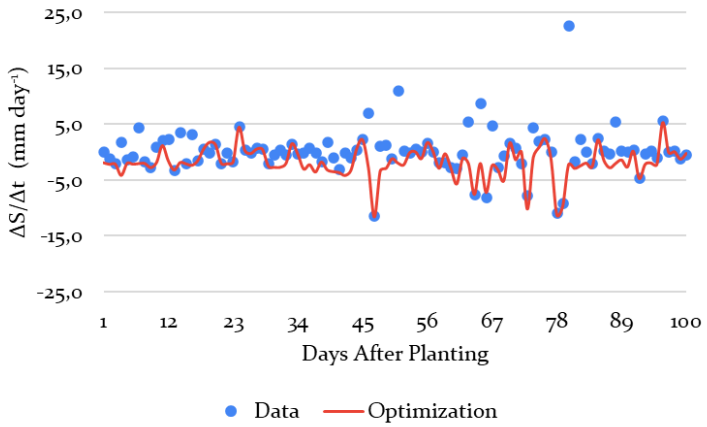


Figure 7. Dynamic of changes in soil water storage

The relatively low coefficient of determination values indicates that the inverse water balance approach is not yet capable of accurately representing the daily variability of changes in soil water storage. This inconsistency may be due to the character of $\Delta S/\Delta t$, which is a numerical derivative of soil water storage, making it highly sensitive to measurement fluctuations and uncertainties in other components of the water balance, such as surface runoff and drainage. In a daily water balance system, small errors in one of the input components can be amplified in the differentiation results, thereby reducing the R^2 value even though the model structure remains conceptually consistent.

Thus, the low coefficient of determination in this soil water storage dynamic does not solely reflect model mismatch but is a consequence of the inverse modeling nature of daily derivative variables that have a low signal to noise ratio. Further evaluation of the temporal consistency and physiological plausibility of the obtained K_c values are more relevant than simply improving the goodness of fit statistical value.

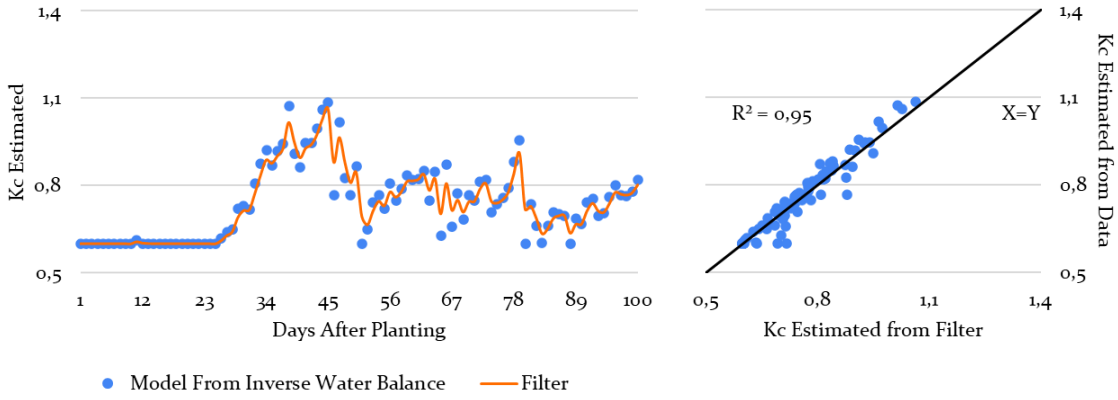


Figure 8. Estimated crop coefficient and Kalman Filter smoothing performance

The water balance reproduced daily storage changes with an R^2 of 0.29 and an *RMSE* of 4.01. Across the series, estimated K_c averaged 0.74, ranging from 0.60 to 1.09 **(Figure 8).** The solution sat on the imposed lower limit of 0.60 on 28 of the 100 days, most of them before flowering. Agreement with the FAO-56 range of 0.60 to 1.20 for rice (Allen *et al.*, 1998) is therefore imposed by the constraint rather than recovered from the data, and we do not present it as corroboration. That the solution rests on the bound for more than a quarter of the season indicates that the unconstrained water balance would place early-season K_c below 0.60, which is consistent with a sparse canopy over a saturated substrate and should be read as a limit of the bounded formulation.

The estimation model was then simplified through smoothing using the Kalman Filter. The inverse water balance analysis was limited by the indicator of the model value approaching the smoothing line. Comparing the raw inverse water balance estimates to the filtered trajectory is an internal consistency check, not an independent validation. Between the raw model outputs and the filtered values, the coefficient of determination was 0.95. At this level of agreement, the Kalman filter smoothed out daily high-frequency measurement noise while maintaining the broader seasonal K_c trend associated with the plants' physiological development. Furthermore, **Figure 9** provides information on the water balance obtained after determining the K_c value.

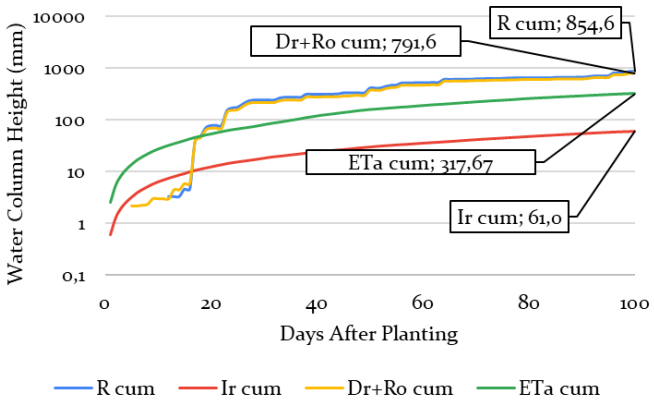


Figure 9. Water balance in the system

In **Figure 9**, the system received 854.6 mm of rainfall and 61.0 mm of irrigation. Combined drainage and runoff totaled 791.6 mm, or 71% of system output, against 317.7 mm of evapotranspiration, giving a storage change of -193.7 mm over the season. Because neither drainage nor runoff was measured individually, their combined total ($D_r + R_O$) was derived alongside K_c within the same optimization. This outflow term is a modeled value rather than an empirical observation, so any error in its estimation propagates directly into K_c. Read with that limitation, the balance indicates that the system discharged most of the water it received during a high-rainfall season, with retention governed by the fixed control level rather than by crop demand.

3.4 Sensitivity and Uncertainty Analysis

Because inverse water balance models rely on unmeasured or imputed parameters, sensitivity and uncertainty analysis is necessary to evaluate how robust the results are (Pianosi *et al.*, 2016). To ensure the model outputs reflect identifiable parameters rather than assumed inputs, we used a one-factor-at-a-time (OFAT) sensitivity approach. This method isolates the effect of uncertainty in each parameter on the final output, helping diagnose specific model constraints in hydrological and environmental systems (Saltelli *et al.*, 2007). The analysis tested four sources of uncertainty: (1) imputed early-season water-level data (Days 1 to 37), (2) parameterization of the Kalman filter noise covariance ratio (Q/R), (3) assumed soil porosity, and (4) uniform daily disaggregation of weekly irrigation volumes.

Missing early-season water-level data. The first test evaluated sensitivity by increasing the imputed water level for Days 1 to 37 by 10% (231 mm rather than 210 mm) and re-solving the water balance. Within the imputed period, daily K_c shifted by at most 8.95% (DAP 31), with 30 of the 37 days shifting by under 5%. These discrepancies carried over into the measured period. Six days after measurements resumed exceeded 10%, reaching 13.21% at DAP 44, 12.15% at DAP 69 and 12.02% at DAP 38 **(Appendix A).** Because the solver estimates K_c, drainage and runoff simultaneously across the full series, changing the initial storage baseline redistributes the downstream partition among these components. Early-season Kc is therefore relatively insensitive to the imputed level, while the late-season trajectory is not, and daily K_c values after Day 37 carry an uncertainty of up to about 13% from this assumption alone.

The second sensitivity test examined the baseline noise covariance ratio ($Q/R = 1, where\ Q = 0.001\ and\ R = 0.001$). Raising this ratio to $Q/R = 10$ caused the filter to track the noisy daily inverse calculations too closely, producing daily K_c deviations of up to 12.45% at DAP 80 **(Appendix B)**. Conversely, lowering the ratio to $Q/R = 0.1$ caused the filter to excessively dampen observation data in favor of the process model, widening the maximum deviation to 15.75% at DAP 51. Furthermore, scaling the absolute magnitudes while maintaining the balanced ratio $Q = 0.01\ and\ R = 0.01$) produced zero deviation (0.00%) from the baseline trajectory. The balanced ratio of 1 was therefore necessary and mathematically robust to damp observation noise while following the gradual phenological development of the crop, regardless of absolute magnitude scaling.

The third sensitivity test evaluated the assumed soil porosity of 68%, chosen to represent typical paddy topsoil. Adjusting this value to 75% and 65% produced maximum daily K_c deviations of 13.21% at DAP 44 and 25.15% at DAP 24, respectively, though most daily estimates varied by less than 5% **(Appendix C).** The identical 13.21% deviation recorded across different perturbation tests at DAP 44 occurs because the solver reached the physiological upper bound of 1.20 (up from a baseline of 1.06), capping further increases. The model remains stable because the inverse water balance relies on the change in soil water storage over time ($\Delta S/\Delta t$) rather than absolute storage volume. Differencing between discrete time steps largely cancels static errors introduced by unmeasured soil properties like total pore space (Vereecken *et al.*, 2008). As long as the timing and magnitude of moisture fluctuations are captured, estimated evapotranspiration fluxes remain insensitive to uncertainties in absolute porosity scaling (Allen *et al.*, 2011). The estimated K_c curve therefore captures crop water demand even without site-specific porosity measurements.

ET-proportional daily disaggregation of irrigation. Although irrigation flow meters were read weekly, weekly volumes were partitioned daily in proportion to potential evapotranspiration (ET_P) rather than divided evenly across the seven days. Because float valves draw water continuously in response to plant uptake, scaling irrigation to atmospheric demand reflects day-to-day transpiration better than an even daily split (Nemali and Van Iersel, 2006). To evaluate how this assumption affects daily K_c estimates, the model was tested against a uniform scenario with weekly totals split equally. Re-solving the inverse water balance under the uniform distribution produced a maximum daily K_c deviation of 11.84% **(Appendix D).** This variation remains minor because irrigation provided only 61.0 mm compared to 854.6 mm of rainfall, representing 6.7% of total water input. Because daily storage changes are governed predominantly by rainfall and actual evapotranspiration, the daily K_c trajectory is robust against sub-weekly irrigation distribution uncertainties.

The final sensitivity test evaluated combined drainage and runoff, which accounts for 71% of total system water output. Because this partition was estimated by the solver rather than measured directly, it is the largest potential source of error. Varying the estimated daily ($D_r + R_o$ values by +10% and -10% forced the model to adjust K_c to close the mass balance. A +10% shift resulted in a maximum daily K_c deviation of 46.37% at DAP 46, while a -10% shift caused a peak deviation of 30.38% at DAP 64 **(Appendix F)**. This high sensitivity indicates that errors in unmeasured outflows propagate directly into the crop coefficient. Future applications of this inverse framework will therefore require direct empirical measurements of drainage and runoff to constrain uncertainty.

3.5 Crop Growth Models and Their Relationship With K_c

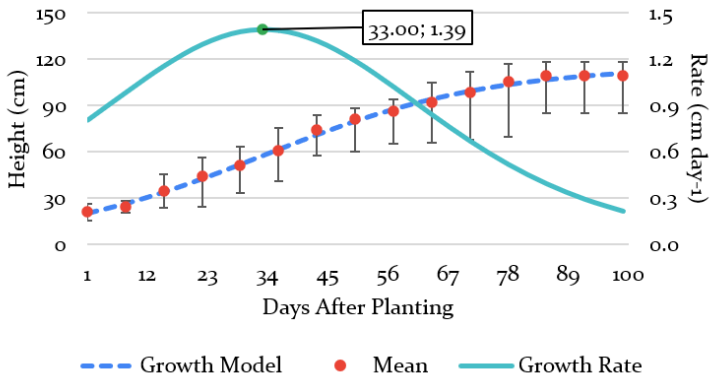


Figure 10. Crop growth model

Figure 10 shows the relationship between rice plant height and growth rate during the observation period. Plant height increased continuously from approximately 25 cm at 1 DAP to about 110 cm at 100 days after planting. The mean observed values closely followed the growth model, indicating that the model adequately described the temporal changes in plant height. The growth rate increased from the beginning of the observation and reached a maximum value of 1.39 cm day^{-1} at 33 DAP, as indicated by the peak of the green curve. This point represents the time when the increase in plant height occurred most rapidly. After 33 days after planting, the growth rate gradually decreased, although plant height continued to increase. The decline in growth rate indicates that the increment in plant height became progressively smaller over time. Toward the end of the observation period, the growth rate decreased to less than 0.3 cm day^{-1}, while plant height approached its maximum value of approximately 110 cm. The close agreement between the observed data and the modelled curve demonstrates that the Verhulst model successfully represented the changes in plant height and the variation in growth rate throughout the observation period. In analyzing the relationship between growth and K_c, a simplification was made whereby the comparison of K_c to plant height was carried out only at system by averaging the growth variables K, A, y, and r. The relationship between growth and K_c can be seen in **Figure 11.**

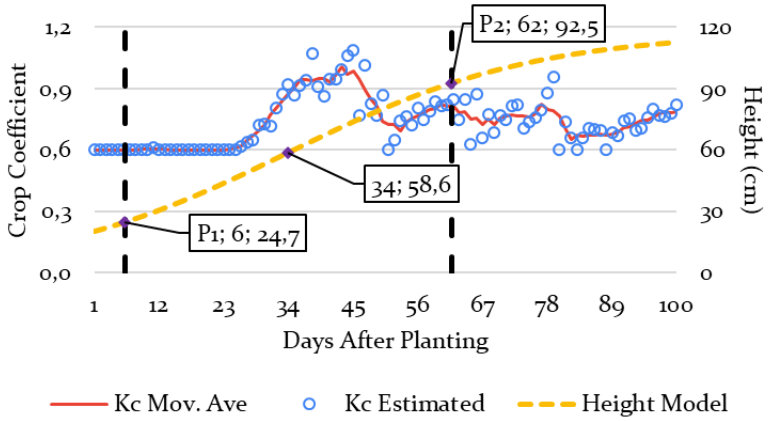


Figure 11. Relationship between crop growth and K_c

Figure 11 provides information about the relationship between crop growth and crop coefficient values. Mathematically, plant growth stages can be divided into three stages, namely the exponential phase, the linear phase, and the ageing phase. The exponential phase lasts from the beginning of growth to point P_1, which is the point where plants experience maximum growth acceleration and the first turning point. The linear phase occurs between point P_1 and points P_2, where the plant experiences maximum deceleration and becomes the second inflection point. Meanwhile, the ageing phase occurs

after passing point P_2 until the end of the growth stage. The positions of P_1 and P_2 are determined based on the inflection point $P_i(t_i, y_i)$, which is marked by $t_i = \frac{\ln A}{r}$ and $y_i = \frac{K}{2}$, where t_1 and t_2 are $t_{1,2} = t_i \pm \frac{1.318}{r}$ and y_1 and y_2 are $0.211K$ and $0.789K$ (Gregorczyk, 1991).

Applying these parameters to **Figure 11**, the specific growth phases is distinctly identified. The exponential phase concludes at point P_1 on day 6 with a plant height of 24.7 cm. The linear phase spans from day 6 to day 62, driven by the maximum growth rate at the inflection point P_i on day 34 at a height of 58.6 cm. The aging phase commences at point P_2 on day 62, where the plant height reaches 92.5 cm.

The dynamics of the Crop Coefficient (K_c) closely tracks these mathematical growth stages. The K_c value increases sharply throughout the linear growth phase between P_1 and P_2. The peak K_c value is achieved shortly after the plants surpass the maximum growth rate at point P_i. Upon passing point P_2 and entering the aging phase, the K_c value decreases and enters a stabilization period.

A Pearson correlation between daily plant growth rate and estimated K_c showed a moderate positive relationship (r = 0.39, n = 100, p = 0.0001). While crop water demand rises alongside rapid growth during the vegetative stage, K_c depends on cumulative canopy cover and phenological stage rather than daily growth rate alone. Each growth phase was therefore analysed separately. The mean and standard deviation of K_c values were calculated for the exponential, linear, and ageing phases. These statistical parameters provide a definitive measure of the K_c variations corresponding to the mathematical growth stages. During exponential phase, the K_c is 0.60 with a standard deviation of 0.00. It increases to 0.75 with a higher standard deviation of 0.15 in the linear phase, reflecting the sharp rise in K_c during the active growth period. In the ageing phase, the mean K_c stabilizes at 0.74 with a standard deviation of 0.08. The highest standard deviation values observed in the linear phase, mathematically correspond to the rapid and continuous increase in crop water demand during the transition from point P_1 to point P_2. Conversely, the lower standard deviations recorded in the exponential and aging phases indicate a more stable K_c value during the initial plant establishment and the final maturation stages.

3.6 Practical Applications and Future Perspectives

The practical deployment of decentralized passive automatic fertigation systems, such as the Nonpowered Automatic Fertigation (FONi) system, offers a highly cost-effective, zero-energy, and scalable alternative to energy-intensive controlled environment agriculture (CEA) configurations in dense urban areas (Huang and Chang, 2021; Daneshyar, 2024). While commercial Plant Factories with Artificial Lighting (PFALs) are heavily constrained by prohibitive capital investments ranging from USD 4.2 to 6.8 million and extreme energy demands of 20 to 50 kWh per kilogram of produce, the passive gravity-fed design of the FONi system operates entirely off-grid (Kumar *et al.*, 2026). This system eliminates grid-energy dependency by utilizing simple float valves and gravity to maintain stable pot water levels. For comparison, while high-tech automated IoT systems remain financially inaccessible to smallholders, semi-automatic or timer-based low-cost drip systems can achieve an exceptionally short investment payback period of just 1.4 planting cycles under resource-constrained conditions in developing nations (Muhammad *et al.*, 2026). FONi requires no grid power and no controller, since float valves and gravity maintain the pot water level. That places its capital and operating requirements below those of controlled-environment configurations such as plant factories with artificial lighting, which carry capital costs of USD 4.2 to 6.8 million and energy demands of 20 to 50 kWh per kilogram of produce (Kumar *et al.*, 2026). We did not cost the system in this study, so its economics remain to be established; the comparison indicates where the savings would arise rather than their size.

In rapidly urbanizing landscapes, such as metropolitan Jakarta, the conversion of fertile agricultural land into residential and industrial zones at an average rate of 650,000 hectares annually poses a direct threat to regional food security (Dinda, 2023). Urban rooftop agriculture (URTA) serves as a vital tool to support household food sovereignty, reduce food transportation distances (food miles), and secure the supply of fresh, nutrient-dense produce close to consumers (Gajbe, 2020). The passive, gravity-fed design of the FONi system reduces labor requirements and simplifies operational management.

Because the crop water supply is regulated automatically by the plant's in-situ consumption, the system minimizes the risk of crop failure due to under- or over-irrigation challenges that frequently limit traditional manual rooftop gardening (Alif *et al.*, 2026). Furthermore, the deployment of such systems supports urban circular economy initiatives; for instance, composted organic municipal solid waste can substitute for commercial substrates, maintaining high crop yields while reducing environmental degradation (Dhika, Widjajani and Maroeto, 2025). When adopted widely, decentralized passive fertigation networks can strengthen community resilience against supply chain disruptions and climate-induced food price shocks (Chythra *et al.*, 2024).

However, converting flat concrete rooftops into active agricultural plots requires careful navigation of building-specific and microclimatic constraints. From an architectural perspective, the structural load-bearing capacity of the building is a primary limiting factor, as saturated soil substrates can exert substantial dead loads of 960 to 1,600 kg/m². The lightweight, containerized design of the FONi system, combined with modern organic substrates, minimizes this structural burden, enabling safe installation on standard residential and institutional flat roofs. Other critical architectural challenges that must be addressed during the design phase include high wind exposure which can dry out soil and damage plant structures, requiring the installation of protective windbreaks or trellises building height constraints, proper waterproofing, and municipal zoning regulations. Despite these constraints, rooftop cultivation yields profound environmental and microclimatic benefits. Bare concrete roofs absorb high amounts of solar radiation, intensifying the urban heat island (UHI) effect. Introducing a vegetated canopy on concrete surfaces absorbs up to 60% of incoming solar radiation through photosynthesis and evapotranspiration (Begum, Kumar Bala and Saiful Islam, 2021). Empirically, rooftop agricultural systems have been shown to reduce localized ambient air temperatures by 1.2 °C to 5.21 °C and bare roof surface temperatures by 3 °C to 12 °C. This thermal buffering dramatically improves building energy efficiency, lowering summer cooling loads. Additionally, integrating rainwater harvesting (RWH) systems can satisfy up to 52.5% to 79.6% of crop water demands, intercepting stormwater runoff and alleviating urban drainage pressure during extreme precipitation events.

While the passive, nonpowered nature of the current FONi system provides an accessible baseline for smallholders, transitioning toward Agriculture 4.0 will require the progressive integration of digital and smart technologies (Chythra *et al.*, 2024; Fei *et al.*, 2025). Future studies should focus on developing low-cost, off-grid electronic monitoring systems. For instance, incorporating low-power microcontrollers (e.g., ESP32 Dev Boards) coupled with capacitive soil moisture, temperature, and pH sensors can provide real-time diagnostic alerts (Alif *et al.*, 2026). Deployed multi-sensor IoT platforms, integrated with lightweight ensemble machine learning models such as Random Forest classifiers, can achieve up to 92% accuracy in predicting crop health and providing context-aware crop recommendations dynamically adjusted to real-time microclimatic conditions. Future research directions must address long-term system performance and biophysical feedback loops. Key areas of investigation include multi-season validation across different seasons to quantify the durability of float valves, calibration drift management (requiring recalibration of pH sensors every 2 to 4 weeks using pH 4.0 and 7.0 buffer solutions to prevent measurement drift from degrading model inputs), and pathogen dynamics in closed recirculating systems where water-borne diseases can propagate quickly. By combining the thermodynamic resilience of passive fertigation with the precision of lightweight digital analytics, smart-adapted urban rooftop farming can become a highly efficient, resource-saving, and scalable pillar of the green cities of tomorrow.

4. Conclusions

Estimating daily crop coefficients (K_c) through an inverse water balance tracked the phenological development of IPB 3S rice under passive fertigation. This provides a basis for day-to-day irrigation scheduling rather than relying on broad growth stages. Several technical limitations qualify these results. The model accounted for observed daily storage changes with an R^2 of 0.29. Evapotranspiration lacked independent measurement, drainage and runoff had to be estimated by optimization, and water levels

were imputed for the initial 37 days. In sensitivity testing, these assumptions shifted daily K_c by as much as 46.4%, primarily reflecting uncertainty in unmeasured outflows. Furthermore, the dataset represents a single cultivar during one season in one rooftop microclimate. The framework demonstrates that estimating daily K_c in rooftop systems is feasible. Even so, the resulting values carry heavy outflow-related uncertainty and should be considered provisional until direct measurements of drainage and runoff can constrain the balance.

Acknowledgement

We would like to express our gratitude to the Ministry of Higher Education, Science, and Technology (KEMDIKTISAINTEK) of the Republic of Indonesia for funding this research under the Pendidikan Magister menuju Doktor untuk Sarjana Unggul (PMDSU) scheme program.

Ethics Statement

This research involved neither human participants nor animals and therefore did not require approval from an institutional ethics committee. All experimental procedures were conducted using rice plants under controlled rooftop cultivation conditions in accordance with institutional research guidelines.

CRediT Author Statement

Baskoro Tri Julianto: Idea Development; Research Design; Investigation; Manuscript Draft Preparation. **Budi Indra Setiawan:** Result Verification; Data Curation; Visualization. **Satyanto Krido Saptomo:** Program Development. **Liyantono:** Formal Analysis. **Euis Kania Kurniawati:** Resources. **Muhamad Askari:** Manuscript Review and Revision.

References

Abdul, L.N.S., Anuar, M.N.A.M. and Mior, A.N.S. 2020. Agriculture management strategies using simple logistic growth model, IOP Conference Series: Earth and Environmental Science, 596(1), p. 012076.

Aimrun, W., Amin, M.S.M. and Eltaib, S.M. 2004. Effective porosity of paddy soils as an estimation of its saturated hydraulic conductivity, Geoderma, 121(3–4), pp. 197–203.

Alamsyar, A. 2022. Dampak alih fungsi lahan padi sawah terhadap ketahanan pangan di kabupaten sigi, agrotekbis: Jurnal Ilmu Pertanian, 10(1), pp. 176–185.

Alif, A.I., Das, S.C., Al-Amin, M. and Hasan, M.M. 2026. Eco sustainable IoT based roof garden monitoring and planting recommendation system with machine learning., Scientific reports [Preprint].

Allen, R.G., Pereira, L.S., Howell, T.A. and Jensen, M.E. 2011. Evapotranspiration information reporting: I. Factors governing measurement accuracy, Agricultural Water Management, 98(6), pp. 899–920.

Allen, R.G., Pereira, L.S., Raes, D. and Smith, M. 1998. FAO Irrigation and Drainage Paper No.56: Crop Evapotranspiration. Rome: FAO - Food and Agriculture Organization of the United Nations.

Arif, C., Setiawan, B.I., Muharomah, R., Ardiansyah, Askari, M., Julianto, B.T. and Erfiana, E. 2025. Fertigator Otomatis Nirdaya (FONi): Teknologi Baru Budidaya Tanaman yang Efektif, Efisien dan Adaptif. 1st ed. Bogor: Penerbit IPB Press.

Azadi, H., Taheri, F., Burkart, S., Mahmoudi, H., De Maeyer, P. and Witlox, F. 2021. Impact of agricultural land conversion on climate change, Environment, Development and Sustainability, 23(3), pp. 3187–3198.

Begum, M.S., Bala, S.K., Islam, A.K.M.S. and Roy, D. 2021. Environmental and social dynamics of urban rooftop agriculture (URTA) and their impacts on microclimate change, Sustainability, 13(16), p. 9053.

Begum, M.S., Kumar Bala, S. and Saiful Islam, A.K.M. 2021. Effect of performance of water stashes irrigation approaches on selected species of plant's water productivity in urban rooftop agriculture with respect to climate change, Water, 14(1), p. 7.

Cascone, S., Coma, J., Gagliano, A. and Pérez, G. 2019. The evapotranspiration process in green roofs: A

review, Building and Environment, 147, pp. 337–355.

Chicco, D., Warrens, M.J. and Jurman, G. 2021. The coefficient of determination R-squared is more informative than SMAPE, MAE, MAPE, MSE and RMSE in regression analysis evaluation, PeerJ Computer Science, 7, p. e623.

Chythra, N.S., Ramya, M., Drishya, N., Radhakrishnan, S., E, N. and Abdul, J. 2024. Recent advancements in aquaponics with special emphasis on its sustainability, Journal of the World Aquaculture Society [Preprint].

Daneshyar, E. 2024. Residential rooftop urban agriculture: architectural design recommendations, Sustainability, 16(5), p. 1881.

Dhika, M., Widjajani, B.W. and Maroeto, M. 2025. Effect of land use on soil water storage in the effective depth (0–60 cm) using the water balance method, Jurnal Teknik Pertanian Lampung (Journal of Agricultural Engineering), 14(6), pp. 2414–2423.

Di Bucchianico, A. 2007. Coefficient of determination (R2), Encyclopedia of Statistics in Quality and Reliability.

Dinda, H.N. 2023. Konsep rooftop greenhouse terintegrasi smart rain water harvesting irrigation sebagai solusi pertanian berkelanjutan di perkotaan, Jurnal Teknologi Pangan dan Ilmu Pertanian, 1(4), pp. 179–190.

Drieschner, M., Herrmann, C. and Petryna, Y. 2023. The data assimilation approach in a multilayered uncertainty space, Modelling, 4(4), pp. 529–547.

Drottberger, A., Zhang, Y., Yong, J.W.H. and Dubois, M.-C. 2023. Urban farming with rooftop greenhouses: A systematic literature review, Renewable and Sustainable Energy Reviews, 188, p. 113884.

Eliades, M., Bruggeman, A., Djuma, H., Christofi, C. and Kuells, C. 2022. Quantifying evapotranspiration and drainage losses in a semi-arid nectarine (Prunus persica var. nucipersica) field with a dynamic crop coefficient (Kc) derived from leaf area index measurements, Water, 14(5), p. 734.

Estinigtyas, W., Suciantini, S. and Irianto, G. 2005. Prediksi curah hujan bulanan berdasarkan suhu permukaan laut nino 3.4 : suatu pendekatan dengan metode filter kalman, Agromet, 19(2), p. 43.

Fei, S., Wu, R., Liu, H., Yang, F. and Wang, N. 2025. Technological innovations in urban and peri-urban agriculture: pathways to sustainable food systems in metropolises, Horticulturae, 11(2), p. 212.

Gajbe, P.U. 2020. Urban rooftop farming – model for sustainable vegetable production and environmental well-being, Agricultural Science Digest - A Research Journal.

Ginoga, V. and Julianto, B.T. 2025. Modeling of labor market dynamics in Balikpapan using the logistic growth model, Jurnal Biometrika dan Kependudukan, 14(2), pp. 158–166.

Gregorczyk, A. 1991. The logistic function - its application to the description and prognosis of plant growth, Acta Societatis Botanicorum Poloniae, 60(1–2), pp. 67–76.

Hargreaves, G.H. and Allen, R.G. 2003. History and evaluation of hargreaves evapotranspiration equation, Journal of Irrigation and Drainage Engineering, 129(1), pp. 53–63.

Hasanah, N.A.I., Setiawan, B.I., Arif, C. and Widodo, S. 2017. "Muka Air Optimum Pada System Of Rice Intensification (SRI)," Jurnal Irigasi, 12(1), pp. 55–64.

Hodson, T.O. 2022. "Root-mean-square error (RMSE) or mean absolute error (MAE): when to use them or not," Geoscientific Model Development, 15(14), pp. 5481–5487.

Huang, A. and Chang, F.-J. 2021. Prospects for rooftop farming system dynamics: an action to stimulate water-energy-food nexus synergies toward green cities of tomorrow, Sustainability, 13(16), p. 9042.

Julianto, B.T., Setiawan, B.I. and Saptomo, S.K. 2024. Box design selection for portable minapadi based on hydrostatic and thermal loading simulation, Jurnal Keteknikan Pertanian, 12(3), pp. 362–375.

Julianto, B.T., Setiawan, B.I., Saptomo, S.K. and Liyantono 2025. Portable Minapadi model and its performance for urban farming, Jurnal Keteknikan Pertanian, 13(2), pp. 195–210.

Julianto, B.T., Setiawan, B.I., Saptomo, S.K., Liyantono and Kurniawati, E.K. 2025. Crop coefficients of paddy and evapotranspiration in the minapadi model system applying nonpowered automatic

fertigation, Jurnal Teknik Sipil dan Lingkungan, 10(2), pp. 319–326.

Kumar, Satendra, Katiyar, H., Kumar, Sunil and Chandra, N. 2026. Urban and vertical farming: productivity, resource efficiency, and scalability in controlled environment agriculture, Journal of Experimental Agriculture International, 48(4), pp. 285–298.

Kurniawan, I., Kristina, L. and Awiyantini, R. 2021. Pengaruh model jarak tanam jajar legowo terhadap pertumbuhan dan hasil padi (Oryza sativa) varietas IPB 3S, Daun: Jurnal Ilmiah Pertanian dan Kehutanan, 8(2), pp. 98–109.

Lodh, A., Routray, A., Dutta, D., Singh, V. and George, John.P. 2024. Impact of <scp>INSAT</scp>-<scp>3D</scp> land surface temperature assimilation via simplified extended Kalman filter-based land data assimilation system on forecasting of surface fields over India, Meteorological Applications, 31(6).

Lopez-Jimenez, J., Vande Wouwer, A. and Quijano, N. 2022. Dynamic modeling of crop–soil systems to design monitoring and automatic irrigation processes: a review with worked examples, Water, 14(6), p. 889.

Maulana, R.A., Warsono, H., Astuti, R.S. and Afrizal, T. 2022. Urban farming: program pemanfaatan lingkungan untuk pengembangan pertanian perkotaan di Kota Semarang, PERSPEKTIF, 11(4), pp. 1329–1335.

Muhammad, H., Rahim, D., N, N., Hamed, A.B.N., Nurul, M. and Kemal, S.A. 2026. Development of a low-cost timer-based drip irrigation system for sustainable Waxy Corn cultivation in El Niño-Prone regions, Open Agriculture, 11.

Muharomah, R., Setiawan, B.I. and Cahrial, E. 2023. Pemberdayaan Kota Tasikmalaya dalam budidaya sayuran menggunakan fertigator otomatis nirdaya (FONi), Jurnal Pengabdian Community, 5(3), pp. 82–87.

Muharomah, R., Setiawan, B.I., Dewi, V.A.K. and Hasanah, N.A.I. 2024. Identification of hydroclimatic patterns and trends in the new capital of Indonesia, BIO Web of Conferences. Edited by Jakaria, 123, p. 04007.

Muharomah, R., Setiawan, B.I. and Suwardi, S. 2024. Diseminasi fertigasi otomatis nirdaya untuk budidaya sayuran di Kota Tasikmalaya, Agrokreatif: Jurnal Ilmiah Pengabdian kepada Masyarakat, 10(2), pp. 156–165.

Nemali, K.S. and Van Iersel, M.W. 2006. An automated system for controlling drought stress and irrigation in potted plants, Scientia Horticulturae, 110(3), pp. 292–297.

Orsini, F., Dubbeling, M., De Zeeuw, H. and Gianquinto, G. (eds.) 2017. Rooftop Urban Agriculture. Cham: Springer International Publishing (Urban Agriculture).

Pianosi, F., Beven, K., Freer, J., Hall, J.W., Rougier, J., Stephenson, D.B. and Wagener, T. 2016. Sensitivity analysis of environmental models: A systematic review with practical workflow, Environmental Modelling & Software, 79, pp. 214–232.

Quasem, M.A. 2011. Conversion of agricultural land to non-agricultural uses in Bangladesh: Extent and determinants, The Bangladesh Development Studies, 34(1), pp. 59–85.

Safitri, D. 2024. Kinerja Fertigator Otomatis Nirdaya (FONi) dengan Irigasi Bawah Permukaan pada Budidaya Padi SRI-Salibu. Thesis. Institut Pertanian Bogor.

Saltelli, A., Ratto, M., Andres, T., Campolongo, F., Cariboni, J., Gatelli, D., Saisana, M. and Tarantola, S. 2007. Global Sensitivity Analysis. The Primer. 1st ed. Wiley.

Saptomo, S.K., Chadirin, Y., Setiawan, B.I., Budiasa, I.W., Kato, H. and Kubota, J. 2015. Quantifying water balance of Subak Paddy Field based on continuous field monitoring, Jurnal Teknologi, 76(15).

Simon, D. 2006. Optimal State Estimation: Kalman, H∞, and Nonlinear Approaches. 1st ed. Wiley.

Vereecken, H., Huisman, J.A., Bogena, H., Vanderborght, J., Vrugt, J.A. and Hopmans, J.W. 2008. On the value of soil moisture measurements in vadose zone hydrology: A review, Water Resources Research, 44(4), p. 2008WR006829.

Weerts, A.H. and El Serafy, G.Y.H. 2006. Particle filtering and ensemble Kalman filtering for state

updating with hydrological conceptual rainfall-runoff models, Water Resources Research, 42(9), p. 2005WR004093.

Ye, J., Zeng, W., Lambert, M., Zecchin, A. and Do, N. 2025. Real-time transient data assimilation in pipe networks using an extended Kalman filter, Cambridge Prisms: Water, 3.